The characteristics of Fe speciation and Fe-binding ligands in the Mariana back-arc hydrothermal plumes

Hu Wang [a,*], Joseph A. Resing [b], Qiaoyang Yan [a], Nathaniel J. Buck [b], Susanna M. Michael [b], Haiyang Zhou [a,*], Meitong Liu [a], Sharon L Walker [b], Qunhui Yang [a], Fuwu Ji [a]

[a] *State Key Laboratory of Marine Geology, Tongji University, Shanghai 200092, P R China*

[b] *Joint Institute for the Study of the Atmosphere and the Ocean, University of Washington and NOAA-PMEL, 7600 Sand Point Way NE, Seattle, Washington 98115, USA*

ABSTRACT

We investigated the speciation of Fe and distributions of Fe-binding ligands in the hydrothermal plumes over high- and low-temperature vents and over diffuse venting fields above the Mariana back-arc spreading center. The concentrations of ligands ([L]) and conditional stability constants (K'_{FeL}) of the natural Fe ligand pool were measured by a reverse titration-competitive ligand exchange-adsorption cathodic stripping voltammetry (RT-CLE-ACSV). The results showed that the buoyant and non-buoyant plume samples over the low-temperature Burke had the highest dissolved Fe/total Fe (DFe/TFe) of 82.2 ± 8.8% and labile Fe/total Fe (Fe_{Lab}/TFe) of 43.3 ± 5.6%. In contrast, in the plume samples above the high-temperature Perseverance field, TFe had the lowest proportions of DFe (48.8 ± 12.2%) and Fe_{Lab} (19.4 ± 8.8%). The linear relationships between Fe species and total Mn (TMn) in the buoyant plume over Burke suggest a simple conservative mixing with ambient seawater, which resulted in constant values of DFe/TFe. However, in the non-

* Corresponding authors.
E-mail address: zhouhy@tongji.edu.cn (H. Zhou), wanghu@tongji.edu.cn (H. Wang)

buoyant plume over Burke, DFe/TFe decreased with plume dilution. The plume samples sourced from the diffuse flow over newly erupted lava had the highest proportion of DFe present as Fe_{Lab} (74.6 ± 4.0%). The [L] in the buoyant plumes over low-temperature Burke vent were up to 113.6 nM, and the $logK'_{FeL}$ decreased with increasing DFe and [L], suggesting the importance of weaker ligands in stabilizing Fe. For all the plume samples, the organically complexed Fe (FeL) constituted significant proportions of the DFe (29.0 ± 9.3%) and Fe_{Lab} (57.5 ± 15.6%) fractions. These Fe-binding ligands were likely sourced from diffuse venting fluids adjacent to the venting sites, and may be also produced by microbes within the hydrothermal plumes.

Keywords: Fe speciation, ligands, RT-CLE-ACSV, Hydrothermal plume, Mariana back-arc

1. INTRODUCTION

Fe is an important and often limiting micronutrient for phytoplankton growth in large areas of the open ocean (Coale et al., 1996). Dissolved Fe (DFe) concentrations are generally very low in surface and deep waters (Boyd et al., 2017). It has been long known that the flux of Fe from hydrothermal vents to the ocean rivals that from rivers (Von Damm et al., 1985), however that Fe was thought to be mostly deposited close to its ridge-crest sources and thus not play a role in the biogeochemistry of the Fe throughout the ocean. Recently, however it has been shown that hydrothermal Fe can be transported throughout the global ocean, making hydrothermal vents an important oceanic Fe source (Fitzsimmons et al., 2014, 2017; German et al., 2016; Nishioka et al., 2013; Resing et al., 2015; Saito et al., 2013; Sander and Koschinsky, 2011; Tagliabue et al., 2010). Global ocean models examining the biogeochemistry of Fe in the ocean require hydrothermal Fe

inputs to describe the distribution of Fe in the ocean (Tagliabue et al., 2010). By using a constant DFe:^{3}He in hydrothermal plumes and global ^{3}He distributions, the model of Tagliabue et al. (2010) was able to demonstrate that hydrothermal Fe impacts global carbon production (Tagliabue et al., 2010; see also Resing et al., 2015). However, the Fe geochemical characteristics (including Fe speciation and DFe:^{3}He) vary in different hydrothermal settings and thus the plumes overlying them (German et al., 2016; Tagliabue et al., 2010). More studies are needed to examine DFe:^{3}He in hydrothermal plumes worldwide. Nearly 40 years of hydrothermal field discovery has revealed more than 630 seafloor hydrothermal fields on mid-ocean ridges and back-arc spreading centers (Baker et al., 2016; Beaulieu et al., 2015). Most hydrothermal studies focus on high-temperature venting (typically 200 ~ 400 °C), however high-temperature venting may only represent a small fraction of the total global hydrothermal heat and mass flux with low-temperature venting (typically < 200 °C) and diffuse flow (typically < 100 °C) being comparatively more important (Bemis et al., 2012; Fornari and Embley, 1995; Mottl, 2003; Rona and Trivett, 1992).

After hydrothermal fluids exit the seafloor, most hydrothermal Fe is precipitated near the hydrothermal vents as sulfide minerals and Fe oxyhydroxides (Mottl and McConachy, 1990). However a substantial portion of Fe remains in the dissolved phase, and can thus influence global Fe budgets and ecosystems (Fitzsimmons et al., 2017; Hawkes et al., 2013a; Sands et al., 2012). Dissolved Fe can be transported thousands of kilometers from venting sites (Fitzsimmons et al., 2014, 2017; Resing et al., 2015), which can influence global Fe budget and carbon export (Ardyna et al., 2019; German et al., 2016; Tagliabue et al., 2016, 2017). The transport of this dissolved Fe is attributed to the presence of organic Fe ligands and nanoparticles in hydrothermal plumes, which

61 facilitate the long-range dispersal of hydrothermal Fe (Bennett et al., 2008; Yücel et al., 2011).

62 It has been demonstrated that 5~96% of DFe exists as colloidal Fe in proximal and distal
63 hydrothermal plume samples (Fitzsimmons et al., 2014; Hawkes et al., 2013a; Sands et al., 2012;
64 Wang et al., 2019). Hawkes et al. (2013a) and Wang et al. (2019) measured the ligands'
65 characteristics in hydrothermal plumes over the East Scotia ridge and Southwest Indian ridge. Both
66 studies suggested that ~30% (on average) of the DFe was bound with ligands, and these ligands
67 stabilized 7.5 ± 7.5% and 12.8 ± 5.4% of the hydrothermal Fe respectively. In open ocean water,
68 more than 99% of DFe is complexed with organic ligands (Gledhill and Buck, 2012).

69 The most common method for determining concentrations of Fe-binding ligands ([L]) and
70 conditional stability constants (K'_{FeL}) of organic Fe complexes in seawater is Competitive Ligand
71 Exchange-Adsorption Cathodic Stripping Voltammetry (CLE-ACSV). This is generally done by
72 titrating the samples with dissolved Fe (forward titration; FT-CLE-ACSV) or additional ligands
73 (reverse titration; RT-CLE-ACSV). In open-ocean waters, where dissolved Fe concentrations are
74 very low (< 2 nM) and [L] > [DFe], FT-CLE-ACSV is the most effective technique, while RT-
75 CLE-ACSV is more effective for water samples with elevated levels of DFe and [DFe] > [L], such
76 as in hydrothermal plumes and coastal waters. To date, only Hawkes et al. (2013a) and Wang et al.
77 (2019) have used RT-CLE-ACSV techniques as the competing ligand to investigate the Fe-binding
78 ligand characteristics in hydrothermal plumes. In both studies, 1-nitroso-2-naphthol (NN) was used
79 as the competing ligand. In this study, 2-(2-thiazolylazo)-p-cresol (TAC) was used as the competing
80 ligand. The use of TAC increases the sensitivity of the voltammetric analyses and reduces the need
81 to precondition titration cells before analysis (Croot and Johansson, 2000).

In this study, we collected hydrothermal plume water samples from the Mariana back-arc above three different areas of hydrothermal activity from November 20 to December 17, 2015, during the expedition FK151121 on board the R/V Falkor as part of the NOAA Earth Oceans Interactions Program Submarine Ring of Fire series of expeditions funded by NOAA's Ocean Exploration and Research Program. The first sampling station was within both a buoyant and non-buoyant hydrothermal plume directly above a known site of low-temperature active venting. The second station was above sites of active diffuse venting directly associated with a recent seafloor eruption (Chadwick et al., 2018). The third station was within the non-buoyant plume produced by a site of high-temperature venting. This study is the first investigation on the characteristics of Fe speciation in hydrothermal plumes over low-temperature venting site, which makes it possible to compare high-temperature venting with the low-temperature and diffuse venting.

2. GEOLOGICAL SETTINGS

This study focuses on hydrothermal venting between 3700m to 4200m along two segments of the Mariana back-arc spreading center. This spreading center is a symmetrically spreading ridge with an arcuate shape nearing the active volcanic arc at both its northern and southern ends. The distance from the arc increases toward its mid-section with separation from the arc being ~110 km at 18°N (Martinez and Taylor, 2003). The two segments discussed here have a slow-spreading ridge morphology and feature axial volcanic rises with smooth volcanic terrain and widespread faulting along the segment centers (Anderson et al. 2017). Anderson et al. (2017) referred to the segments studied here as tectonic segments undergoing magmatic extension.

The segment centered at 15.5°N experienced a recent eruption (months to several years) prior to our sampling with 36.5 m thickness lava flows on the seafloor between 15.4°N and 15.5°N (Chadwick et al 2018). Near the axial high, north of the new lava flows, conductivity-temperature-depth (CTD) tow-yo (cycling the CTD package up and down behind the ship only through the bottom few hundred meters) and autonomous underwater vehicle (AUV) *Sentry* plume data provided evidence for high-temperature venting between 15.47 and 15.54 °N, and ROV dives in 2016 located a high temperature vent field with maximum temperature of 265.7°C at 15.48°N, 144.51°E that was named Perseverance vent field (Butterfield et al., 2017). CTD tow-yos and *Sentry* mapping suggest that other vent sources must be present on the segment high (Baker et al, 2017).

On the segment centered at 18.2°N CTD tow-yos identified numerous sites of hydrothermal activity at the axial highs including a collection of three vents named Alice Springs, Illium, and Burke located within several km of each other. High temperature venting (>267°C) has been observed at these sites previously (Campbell et al., 1987; Gamo et al., 1997; Hessler and Londsdale, 1991). However, a CTD tow-yo and *Sentry* dive during our cruise in 2015 recorded weak Nephelometric Turbidity Units (ΔNTU < 0.01) in non-buoyant plume above Burke (Baker et al., 2017; Resing et al., 2016), and ROV dives in 2016 found extinct chimneys and low-temperature (< 51°C), clear fluids being emitted at Burke (Butterfield et al., 2017). The agreement between these observations implies that the Burke vent has changed from a high-temperature to a low-temperature vent.

3. MATERIAL AND METHODS

3.1. Sample collection

Hydrothermal plume water samples were collected from two CTD tow-yos, T15B-06 (hereby referred to as T6) and T15B-09 (hereby referred to as T9), and a vertical CTD cast - V15B-02 (hereby referred to as V2) in the South Mariana back-arc (Fig. 1). V2 and six T9 samples were collected in the buoyant and non-buoyant plume respectively over the active Burke hydrothermal field at 18.18°N, 144.70°E (Fig. 2). T6 was conducted along the axis from 15.40° to 15.58° N (Fig. 3). The southern portion of this tow-yo was conducted just above a new lava flow and the northern portion was associated with focused high-temperature venting in the Perseverance field (Baker et al., 2017; Chadwick et al, 2018). The hydrothermal plumes were detected and sampled using a CTD profiler system combined with optical backscatter and oxidation-reduction potential (ORP) sensors that were mounted on a stainless steel frame with 21 trace metal clean 17.5 L Niskin-style sampling bottles with epoxy-coated springs. Plumes were identified and sampled based on positive turbidity and negative ORP anomalies. Upon recovery, samples for total Fe (TFe) and Mn (TMn) analysis were collected directly from the sampling bottles into clean low density polyethylene bottles (LDPE, Nalgene) and acidified to pH < 2 with sub-boiling distilled HCl. Then, the Niskin bottles were pressurized to enable the passage of samples through Supor membrane (0.2 μm) filters (Pall Inc.) into LDPE bottles. The filtered water was stored immediately at -20°C until analysis. A subset of filtered samples was collected and acidified for dissolved Fe and Mn analysis.

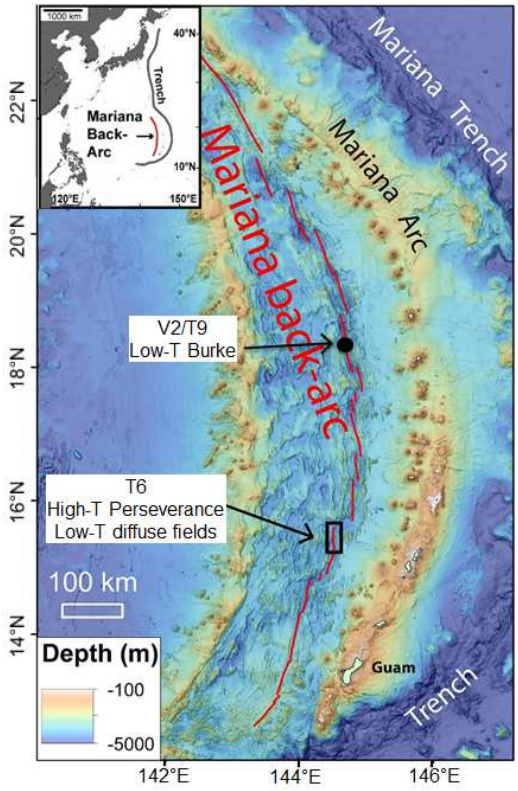

Fig. 1. The locations of T6, T9 and V2, "Temperature" was abbreviated to "T" (Figure based on Chadwick et al., 2018).

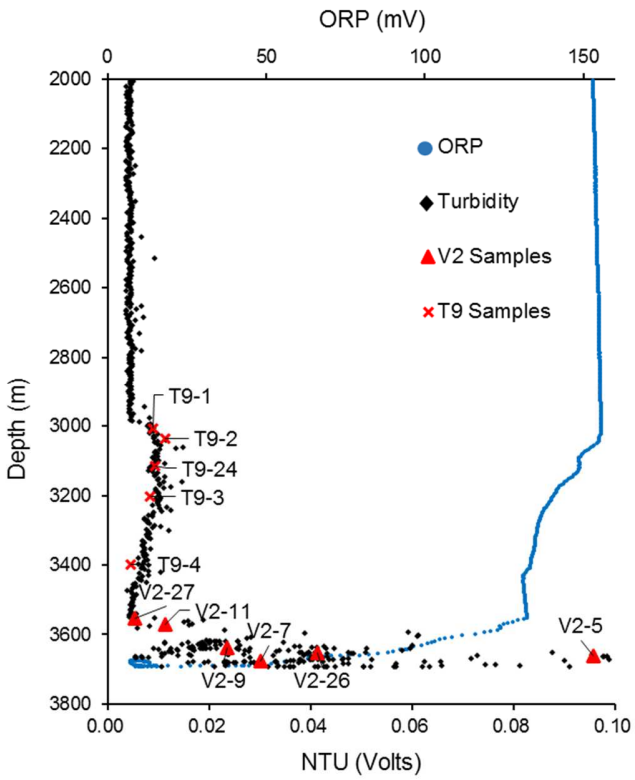

Fig. 2. Turbidity signal, ORP data and the locations of V2 (buoyant plume) and T9 (non-buoyant plume) samples collected over Burke.

3.2. Determination of Fe-binding ligands

The modified RT-CLE-ACSV method used here is similar to that described by Hawkes et al. (2013b) and Wang et al. (2019) for Fe and Nuester and van den Berg (2005) for Cu. Here, we used TAC instead of NN as the ligand that competes with natural ligands present in the sample. TAC is a more sensitive competing ligand for Fe than NN (Croot and Johansson, 2000). The sensitivity of $Fe(TAC)_2$ in this study was determined to be ~ 6.7 nA nM^{-1} min^{-1} compared to ~ 0.7 nA nM^{-1} min^{-1} for $Fe(NN)_3$ without any catalyst. The formed $Fe(TAC)_2$ is determined by ACSV. K'_{FeL} and [L] are calculated by modeling the titration data as discussed below.

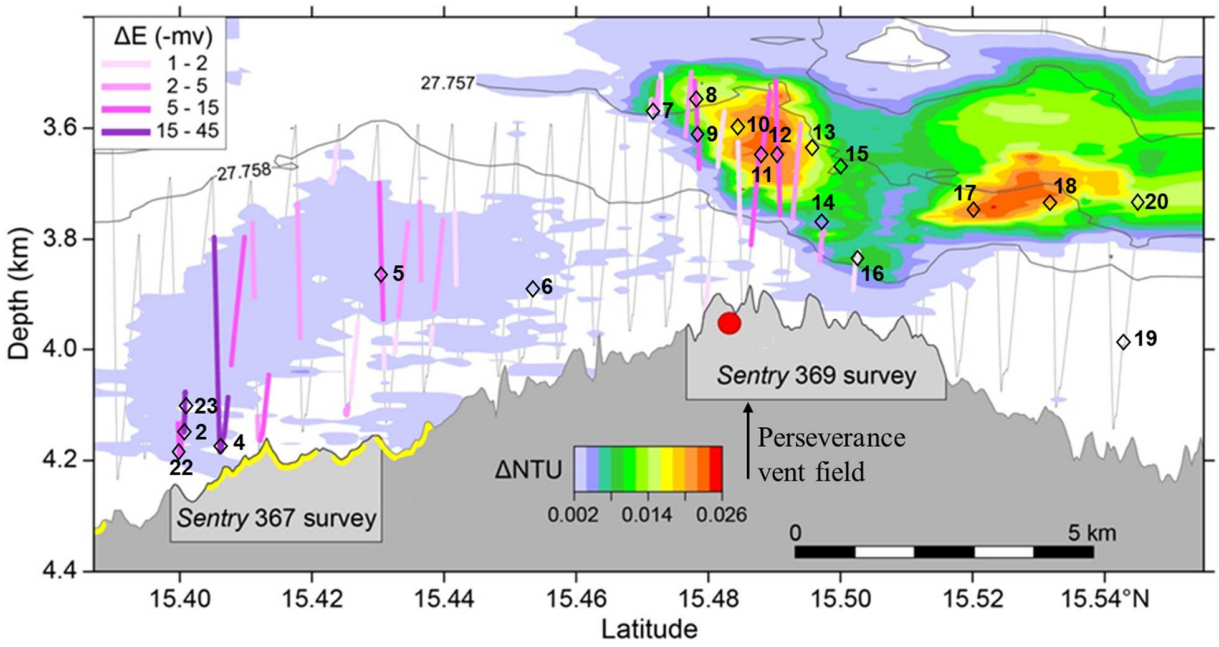

Fig. 3. The particle anomalies (ΔNTU) and ORP distributions above the Mariana back-arc segment centered at 15.5°N from CTD tow-yo T6. The gray line shows the tow-yo trackline, while the hollow diamonds are bottle sample locations with labels indicating Niskin bottle number. Colored lines along CTD tow-yo path show ORP anomalies (ΔE). Yellow highlight on the bathymetry profile indicates areas of new lava. The red dot shows the location of Perseverance vent field (Figure based on Baker et al., 2017 and Chadwick et al., 2018).

3.2.1. Apparatus and reagents

Voltammetric experiments were carried out using a 797 VA Computrace (Metrohm) equipped with a hanging mercury drop working electrode, Ag/AgCl reference electrode and platinum auxiliary electrode. The sample manipulations were performed in an Airclean 100 laminar flow bench. All the titration experiments were performed in an acid-cleaned PFA cell. Sample bottles (LDPE, Nalgene) and the PFA titration vials (30 mL) were first cleaned by a 1:4 acetone to ethanol mixture and then soaked in 60°C 1.2 M HCl for at least 4 days.

Stock solutions (0.1mM, 1mM and 10mM) of TAC (Sigma Aldrich) were prepared by

dissolution in HPLC grade methanol (Thermo Fisher Scientific) and stored at 4°C when not in use. A 1.0 M N-(2-hydroxyethyl) piperazine-N′-2-propanesulfonic acid (EPPS, Sigma Aldrich) buffer solution was prepared in 1.0 M ammonium hydroxide (Sigma Aldrich). The addition of 75 µL EPPS buffer to 15 mL seawater yielded a final pH = 8.0. This EPPS solution was purified by equilibrating with Chelex 100 resin (Bio-Rad) for 24 h. Fe standards were prepared from hydrated $FeCl_3$ (Sigma Aldrich) in 1% quartz distilled HCl.

3.2.2. Procedure for determining Fe-binding ligands

The theory and procedure of reverse titration have been described in Hawkes et al. (2013b). In brief, water samples were thawed and vigorously shaken to ensure uniform mixing before analysis. Then, subsamples (15 mL) were pipetted into 12 polytetrafluoroethylene (PTFE) vials. EPPS (75 µL) was added to each vial. Variable amounts of stock TAC solution (0.1, 1, 10 mM) were added to 12 vials, to yield final concentrations ranging from 0.2 to 40 µM TAC in the vials. These solutions were allowed to equilibrate overnight, typically > 15 h. The samples were then transferred to the PFA cell, and purged with nitrogen for 180 s followed by the determination of $Fe(TAC)_2$ by CSV in differential pulse mode. The deposition potential was -0.4 V for 180 s and the solution was stirred continuously during the analysis. After a quiescence period of 10 s, the current was monitored as the potential was scanned from -0.4 V to -0.9 V at 50 mV/s. The modulation amplitude was 50 mV. The labile Fe (Fe_{Lab}) was obtained at the highest TAC concentration (40 µM) by standard addition of Fe.

The concentration of natural ligands in a sample ([L]), and their conditional stability constants,

184 K'_{FeL} were determined by fitting the parameters (K'_{FeL} and [L]) in equation 1 and minimizing the
185 sum of squared differences between the values of X ($X = i_p/i_{pmax}$) obtained during the titration and
186 the modeled values of X (From Eq. 1) using an Excel spread sheet and the Excel Solver tool.

187 $$X=(1-j)\frac{\alpha_{Fe(TAC)_2}}{\alpha_{Fe(TAC)_2}+\alpha_{Fe'}}+j\frac{\alpha_{Fe(TAC)_2}}{\alpha_{Fe(TAC)_2}+\alpha_{Fe'}+\sum_i\frac{K'_{FeL_i}[L_i]}{1+K'_{FeL_i}[Fe^{3+}]}} \quad (1)$$

188 Where j is the ratio (0~1) of [L] to [Fe_{Lab}] and $\alpha_{Fe(TAC)_2}$ represents the side reaction coefficient
189 of TAC and is given by $\alpha_{Fe(TAC)_2}=\beta_{Fe(TAC)_2}[TAC]^2$, where $\beta_{Fe(TAC)_2}$ is the binding strength of
190 $Fe(TAC)_2$ and obtained by titrating UV digested seawater (see Appendix). $\alpha_{Fe'}$, the inorganic Fe
191 side reaction coefficient, varies with pH, temperature and ionic strength (Liu and Millero, 2002;
192 Millero and Pierrot, 2007). We used equations from Millero and Pierrot (2007) to calculate $\alpha_{Fe'}$ at
193 various salinities at pH=8.0, with a value of 1.23×10^{10} at S=34.6 (salinity of Mariana samples). An
194 example output for Sample V2-11 can be found in Appendix (Fig. S1).

195 Although two ligand classes have been detected in coastal areas (Buck et al., 2007; Bundy et
196 al., 2014), the use of a one-ligand model produces similar results as the two-ligand model which
197 indicates very low concentrations of stronger ligands. As a result, in this study, the unit of the ligand
198 concentration, "nM", is actually "nM Fe equivalent". However, it should be noted that the binding
199 strengths of different ligand classes are related to the detection windows of different analytical
200 methods and the associated data treatments, and that the modelled conditional stability constants
201 and concentrations represent the average values of multiple Fe-binding ligands present in any given
202 sample (Gledhill and Buck, 2012).

203 **3.3. Determination of TFe and DFe**

In order to determine DFe concentrations, acidified seawater samples were UV irradiated for two hours in precleaned quartz tubes. These samples were brought to pH=8.0 with Q-NH_4OH and analyzed for DFe by the CSV method as described in Section 3.2.2. TFe (unfiltered) and a subset of DFe samples were collected and acidified to pH < 2 and were determined by flow injection method from Measures et al. (1995) in the NOAA's Pacific Marine Environmental Laboratory (PMEL). DFe concentrations determined by the two methods agreed well (excluding sample V2-26). The replicate analyses (n=6) of NASS-6 (National Research Council of Canada) averaged 8.62 ± 0.28 nM, which corresponds well with the certified value of 8.84 ± 0.82 nM. The detection limit of Fe for 180 s deposition at 40 μM of TAC was 0.2 nM (3 times the ratio of signal-to-noise).

3.4. Determination of TMn and DMn

TMn and DMn were determined by direct-injection flow injection analysis (Resing and Mottl, 1992) as modified by Resing et al. (2009) at NOAA's PMEL. The replicate analyses (n=10) of standards indicated the precision of TMn and DMn is ± 1nM or 3% (whichever is greater). The accuracy of Mn measurement was assured by running an internal standard (25.2 ± 0.7 nM) at least once daily.

4. RESULTS

4.1. Hydrothermal Plume Characteristics

Hydrothermal activity along the Mariana arc was discussed extensively by Baker et al. (2017). The northern section consists of a known venting site, the low-temperature Burke Vent field

(Campbell et al., 1987; Hessler and Londsdale, 1991; Ishibashi et al. 2015), while the southern section is divided into a section recently perturbed by a submarine eruption and a section closer to the axial high hosting high temperature venting.

The eruptive section (15.40 to 15.46°N) was overlain by a continuous, but weak particle plume (ΔNTU < 0.005) that was present throughout the water column from the seafloor to ~400-500 m above bottom (Fig. 3). Pervasive ORP anomalies were observed near the seafloor throughout the CTD tow-yo and visual observations during a Sentry AUV dive confirmed widespread discharge of low-temperature diffuse fluids associated with the new lava flows (Baker et al., 2017; Chadwick et al., 2018). The northern Mariana Back Arc basin is isolated below 3000 m and below this depth the density gradient was very slight and thus any higher temperature focused fluids would be expected to rise up higher in the water column.

The hydrothermal plumes located above the axial high (15.5°N) exhibited higher particle anomalies (~ 0.025 NTU) and Fe and Mn concentrations that were ~ 2 x higher than that observed on the eruptive section. From the measured turbidity and ORP anomalies (Fig. 3), the samples of T6 (except 6 DF samples) collected here may come from at least two separate non-buoyant plumes over high-temperature Perseverance venting field.

Above Burke vent field, the actively buoyant and non-buoyant plume samples were collected during CTD vertical cast V2 and CTD tow-yo T9. The buoyant plume samples (V2) had particle and ORP anomalies (ΔNTU = 0.12, ΔE = 150 mV) (Fig. 2), and changes in potential temperature ($\Delta\theta$ = 0.36°) within the bottom 25 m. The non-buoyant plume samples of T9 had weak particle anomalies (ΔNTU = 0.01), ORP anomalies (ΔE = 30 mV) and no temperature change (Fig. 2).

4.2. TMn and DMn in hydrothermal plumes

TMn concentrations were significantly higher in the buoyant plume samples above Burke, ranging from 87.9 nM to 1148.3 nM, compared to those in other plume samples that had concentrations ranging from 8.6 nM to 32.6 nM (Table S1). It is apparent that Mn existed almost entirely in the dissolved phase in all samples, with DMn making up 104 ± 4% of TMn, suggesting that the ratio of particulate Mn to TMn was negligible. This is consistent with the near-conservative behavior of Mn within hydrothermal plumes close to the vent sources due to the slow oxidation rate of Mn (days to weeks) (Dick et al., 2009; James and Elderfield, 1996; Sands et al., 2012). Therefore, it is reasonable to use Mn as the tracer of plume dilution in this study.

4.3. Fe speciation in the hydrothermal plumes

Over the low-temperature Burke vent, TFe, DFe and Fe_{Lab} in the V2 buoyant samples ranged from 41.4 nM to 457.5 nM, 37.2 nM to 394.8 nM and 19.6 nM to 152.0 nM respectively, which were higher than those in other samples (Table S1). As the buoyant plume rises, it entrains surrounding seawater until eventually becoming non-buoyant after which it spreads laterally. The six samples from T9 samples that were collected in this non-buoyant plume had substantially lower concentrations of [TFe], [DFe] and [Fe_{Lab}] compared to those in the buoyant portion of the plume (Table S1). The TFe, DFe and Fe_{Lab} correlate with each other (Fig. 4), suggesting they all originated from hydrothermal venting.

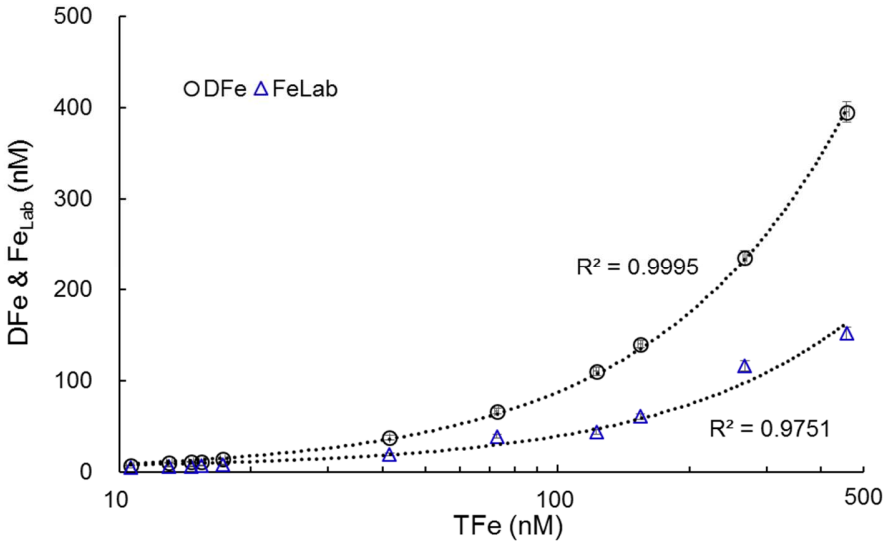

Fig. 4. The relationships between DFe, FeLab and TFe in plume samples over the Burke vent. Error bars represent ±1 standard deviation of two replicate analyses. Most error bars are smaller than the symbols in size.

In the plume samples at the axial high over high-temperature Perseverance field, the concentrations of TFe, DFe and Fe_{Lab} varied from 16.3 nM to 99.6 nM, 7.7 nM to 42.2 nM, 3.8 nM to 16.3 nM respectively (Table S1). About half of the TFe on average was present as DFe, 48.8 ± 12.2% (Table. S2). These results are comparable with previous reports (Hawkes et al., 2013a; Kleint et al., 2016; Wang et al., 2012, 2019).

In the low-temperature diffuse flow samples collected from above the new lava flows, TFe, DFe and Fe_{Lab} concentrations ranged from 27.9 nM to 61.2 nM, 13.4 nM to 23.6 nM and 9.5 nM to 18.6 nM respectively (Table S1). TFe was 44.4 ± 3.7% DFe and 33.2 ± 3.6% Fe_{Lab} (Table S2), which were similar to those in the neighboring plumes over high-temperature Perseverance venting field.

4.4. Fe ligands in hydrothermal plumes

The conditional stability constants of the natural ligands ($logK'_{FeL}$) found in all of the samples were between 19.25 ± 0.11 and 20.54 ± 0.14 (Table S1) with no significant difference between

277 samples from low- and high-temperature vent fields and from diffuse flow. The [L] in the plume
278 samples above the low-temperature Burke vent varied from 2.4 nM to 113.6 nM (Table S1), and
279 were significantly higher than those in the plumes along the southern segment, which ranged from
280 1.8 nM to 12.1 nM. DFe and Fe_{Lab} exceeded [L] in all samples. This result is consistent with
281 previous studies on Fe-binding ligands in hydrothermal plumes (Bennett et al., 2008; Buck et al.,
282 2015; Hawkes et al., 2013a; Wang et al., 2019).

283 **5. DISCUSSION**

284 **5.1 The RT-CLE-ACSV method using TAC as the competing ligand**

285 The modelled stability constants (K'_{FeL}) and ligand concentrations ([L]) are related to the
286 detection window of CLE-ACSV method, which is defined by the side reaction coefficient of the
287 competing ligand ($\alpha_{Fe(TAC)_2} = \beta_{Fe(TAC)_2}[TAC]^2$ in the case of TAC, $\alpha_{Fe(NN)_3} = \beta_{Fe(NN)_3}[NN]^3$
288 in the case of NN). At the highest concentration of TAC or NN, 40 μM, $\alpha_{Fe(TAC)_2}$ ($10^{12.8}$) is
289 slightly lower than $\alpha_{Fe(NN)_3}$ ($10^{13.5}$). This might be the reason that $\log K'_{FeL}$, 19.91 ± 0.39,
290 measured in this study are comparatively lower than that reported by Hawkes et al. (2013), 20.61
291 ± 0.54, and Wang et al. (2019), 20.36± 0.46, which used NN as the competing ligand, although
292 there is no significant difference between them.

293 Laglera et al. (2011) has noted that CLE-ACSV with either NN or TAC can't detect humic
294 substances due to out-competition of NN and interactions of TAC with humic substances functional
295 groups. Most humic substances have a terrestrial origin and are abundant in coastal waters (Laglera
296 and van den Berg, 2009), and concentrations typically decrease from shore to sea. It was shown

297 that the percentage of Fe complexation by humic substances in the San Francisco Bay decreased
298 from 23% at salinity 4.2 to 3% at salinity 33.9 (Bundy et al., 2015), suggesting that they may only
299 constitute a small part of dissolved organic matter in the deep-sea (Bundy et al., 2015; Laglera and
300 van den Berg, 2009). In fact, deep-sea humic substances may be different from those in coastal
301 waters, and as a result, may have different impacts on CSV measurements. Several studies
302 suggested that there was no significant difference in the Fe-binding capacity in the deep water of
303 the north Pacific Ocean despite using 2,3-dihydroxy-naphthalene (DHN), salicylaldoxime (SA) or
304 TAC as the competitive ligand (Kondo et al., 2012; Laglera and van den Berg, 2009; Rue and
305 Bruland, 1995). Consequently, the underestimation of Fe-binding ligand concentration might be
306 insignificant, and more studies are needed to elucidate the interactions between TAC and humic
307 substances in deep seawater.

308 **5.2 The difference of the Fe speciation in plumes over low- and high- temperature vents**

309 **5.2.1 The proportions of DFe and Fe_{Lab}**

310 In both the buoyant and non-buoyant plume samples over Burke, 82.2 ± 8.8% of Fe was present
311 as DFe of which 53.3 ± 9.2% was labile (Fe_{Lab}; Table S2). This suggests that most of the DFe may
312 be present as weakly crystalline Fe-oxyhydroxides and organic Fe complexes (Hawkes et al., 2013a,
313 2014). On the contrary, in the plumes over the high-temperature Perseverance field, DFe was only
314 48.8 ± 12.2 % of TFe and Fe_{Lab} was 38.8 ± 10.0% of DFe (Table S2). This suggests that less of the
315 DFe is accessible by the added TAC ligand. Instead DFe may be composed of more crystalline Fe
316 sulfides, oxides and/or more of it may be bound by very strong ligands that are undetectable due

317 to the comparatively weak binding strength of the competing TAC ligand (Hawkes et al., 2013a,
318 2014). However, the Fe_{Lab} concentrations determined using the stronger competitive ligand, NN,
319 were similar with that using TAC (Table S1), suggesting that Fe bound with natural ligands stronger
320 than TAC might be not important.

321 In previous studies, DFe that was found to constitute more than 80% of TFe in hydrothermal
322 plumes above high-temperature vents was ascribed to the low pH and dissolved oxygen
323 concentrations in the Pacific Ocean resulting in slow rate of Fe(II) oxidation (Field and Sherrell,
324 2000). In the Mariana Back Arc, difference in pH and dissolved oxygen concentrations between
325 Burke and Perseverance vent fields should be small since the sites are relatively close to one
326 another and are at similar depths. In view of the clear, shimmering and particle-free fluids issuing
327 from Burke (Butterfield et al, 2017), we speculate that the low-temperature venting and low
328 concentration of H_2S in Burke fluid might explain the high value of DFe/TFe and Fe_{Lab}/DFe, which
329 resulted in less Fe sulfides and more acid soluble Fe in the dissolved phase. Hawkes et al. (2014)
330 also observed 64.8 ± 8.1% of DFe/TFe and 36.7 ± 21.3% of Fe_{Lab}/DFe in the hydrothermal plumes
331 over high-temperature island arc venting fields in the eastern Scotia Sea of the Southern Ocean, in
332 which Fe sulfides were also a minor component in the plume samples.

333 **5.2.2 The relationships between TFe, DFe, Fe_{Lab} and TMn**

334 TFe, DFe and Fe_{Lab} in plume samples over Burke correlate with TMn. However, buoyant and
335 non-buoyant samples show different trends versus TMn (Fig. 5). The different Fe species show a
336 better correlation with TMn in the buoyant versus non-buoyant plumes (Fig. 5), which suggests

337 simple conservative mixing between the vented hydrothermal fluids and surrounding seawater in
338 the buoyant plume. This result is somewhat surprising as we would expect Fe loss in the near field
339 buoyant plume (Mottl and McConachy, 1990). This is supported by the particle and sulfide poor
340 fluids venting from the seafloor, which makes Fe removal as sulfide less likely. It may be that Fe
341 from low-temperature venting is more readily preserved during plume formation; the absence of
342 other comparable data published for plumes above low-temperature venting makes the global
343 application of this observation difficult. Future investigations into the Fe preservation in plumes
344 above low-temperature vent fields are strongly recommended. In addition, we found that DFe/TFe
345 ratios in the buoyant and non-buoyant plumes behave differently with plume dilution (Fig. 6A). In
346 the buoyant plume samples, DFe/TFe is almost constant due to the conservative mixing. While it
347 decreased as the non-buoyant plume mixed with seawater, it decreased only ~15% on average in
348 these samples (Fig. 6A). It may be related to the transfer of DFe into particulate Fe according to a
349 recent investigation of Fe species in hydrothermal plumes (Lough et al., 2019). However, our
350 present data cannot prove it directly.

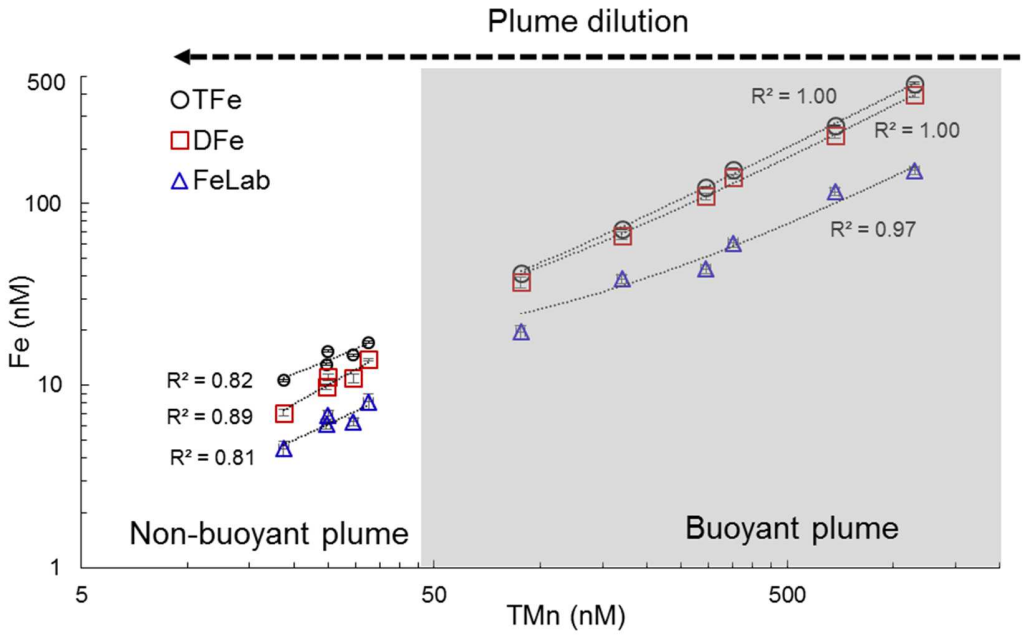

Fig. 5. The correlations between DFe, Fe_{lab}, TFe and TMn of V2 (buoyant plume) and T9 (non-buoyant plume) samples. Error bars on TFe, DFe and Fe_{Lab} concentrations represent ± 1 standard deviation of two replicate analyses. Error bars on TMn concentrations represent 3% standard error based on standard reproducibility.

In contrast to the plumes above Burke, the non-buoyant plume samples above the high-temperature Perseverance field displayed weak correlations between TFe, DFe, Fe_{Lab} and TMn. It might be related to the high-temperature venting, which led to high concentrations of Fe dissolved in fluids and greater loss or precipitation of Fe after the fluids were expelled from the seafloor and mixed with ambient seawater (Bennett et al., 2009; Hawkes et al, 2013a; Kleint et al., 2016; Sands et al., 2012). Another reason might be related to the possibility that the plumes that were sampled came from different sources. Additionally, we didn't collect the buoyant plume samples above Perseverance field.

Recently, Lough et al. (2019) investigated Fe species in both the buoyant and non-buoyant plume samples over the Beebe Vent Field located on the Mid-Cayman Spreading Center, Caribbean

Sea, which is a high-temperature vent field (393 - 401 °C). They showed DFe/TFe increased during ascent of the buoyant plume (Fig. 6B). This was ascribed to extensive precipitation and loss of Fe sulfides and oxyhydroxides close to the vent, thus resulting in the decrease of TFe. In the non-buoyant plume, the DFe/TFe decreased as plume dispersed. This trend is similar with our result of DFe/TFe in the non-buoyant plume over low-temperature Burke, however their values of DFe/TFe are relatively lower and comparable with that above high-temperature Perseverance field. Further, Lough et al. (2019) investigated the colloidal fraction of Fe and indicated that the decreasing of DFe in the non-buoyant plume samples resulted from the transformation of colloidal Fe into particulate Fe. Another study of Bennett et al. (2009) investigated the DFe and TFe change in a buoyant hydrothermal plume at 5°S Mid-Atlantic Ridge. They also observed that DFe/TFe increased during ascent of the buoyant plume.

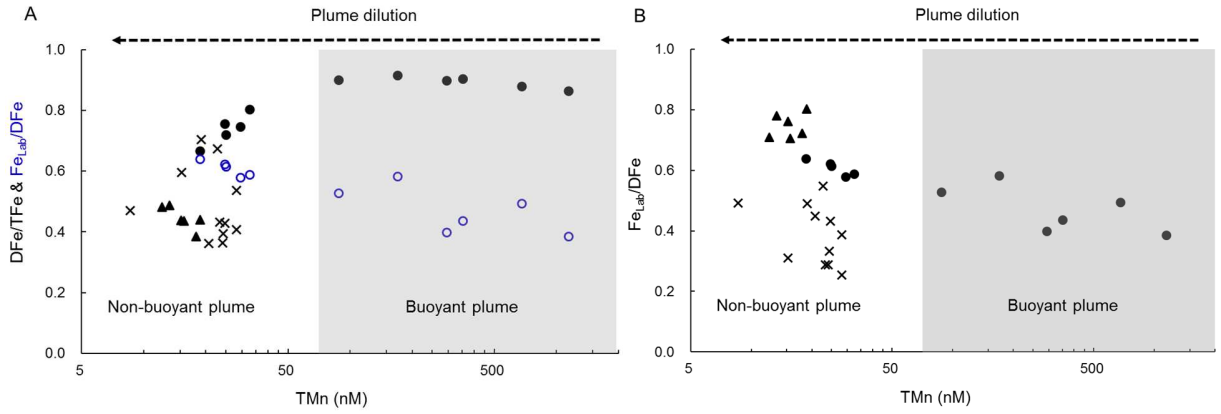

Fig. 6 A - DFe/TFe changes in the plume samples above Burke (black circles), Perseverance (black crosses) and diffuse venting fields (black triangles); Fe_{Lab}/DFe changes in the plume samples above Burke (blue circles). B – DFe/TFe change in the plume samples over the Beebe Vent Field, Caribbean Sea (data from Lough et al., 2019).

Intriguingly, we found that the Fe_{Lab} increased slightly relative to TMn from the buoyant to

non-buoyant plumes over Burke (Fig. 5A), which is contrary to the decrease of DFe/TFe. The likely reason may be that it was the non-labile Fe in DFe (e.g. crystalline Fe oxyhydroxides and sulfides) that aggregated into particulate Fe, while the labile Fe was comparatively stable in the dissolved phase. This is also consistent with the high proportions of stable organically complexed Fe in Fe_{Lab} (Table S2).

5.3 Fe speciation in diffuse flow plumes over newly erupted lava

Six plume samples were collected over a young lava-flow with wide-spread low-temperature diffuse venting. These samples revealed positive correlations between TFe, DFe and Fe_{Lab} and each with TMn. These observations are generally similar to those in the low-temperature Burke plumes. The most noticeable feature of the distributions of Fe species in these plume samples is that the proportions of DFe present as Fe_{Lab} were higher than that observed elsewhere along the back arc, averaging 74.6 ± 4.0% (Table S2). We suspect this must be related to the low-temperature diffuse venting and that the venting was associated with the lava flows that were only several months old before sampling (Chadwick et al., 2018). The formation of rich and diverse biological communities had not taken place as confirmed by ROV dives in 2016 (Butterfield et al., 2017). Consistently, the organic Fe ligand fraction of Fe_{Lab} ([L]/Fe_{Lab} in Table 2) in these diffuse flow samples was not higher than that in other samples (Table S1 and S2). Considering that Fe_{Lab} mainly includes organic Fe complexes and weakly crystalline mineral phases (e.g. Fe oxyhydroxides), we therefore speculate that the high Fe_{Lab}/DFe in the diffuse flow over the new lava must be due to the high concentrations of small, poorly crystalline Fe oxyhydroxides. It is possible that very low concentrations of vented Fe combined with dilution with ambient seawater may result in the

formation of these small or poorly crystalline colloids. Only Kleint et al. (2016) have analyzed Fe_{Lab} in one diffuse venting fluid sample and their results showed only 1.1% of DFe was Fe_{Lab} (= 5 nM). However, they proposed that the proportion of Fe_{Lab} may increase as the plume was diluted due to the removal of non-labile Fe, although they didn't measure Fe_{Lab} in the overlying plumes.

5.4 The characteristics and sources of the Fe-binding ligands in hydrothermal plumes

Previous work and speciation models have reported that high DFe concentrations might result in high [L] and ligands with low stability constants. It is thought that strong ligands bind with Fe first, especially at low DFe concentrations, while weaker ligands progressively contribute to complexation at higher DFe concentrations in organic rich seawater (Croot and Heller, 2012; Gerringa et al., 2007; Gledhill and Gerringa, 2017; Kleint et al., 2016; Town and Filella, 2000). The conditional stability constants, K'_{FeL}, in this study were indeed comparatively lower than those of most Fe complexes reported in deep oceans with very low Fe concentrations using the forward titration method (Buck et al., 2015; Gledhill and Buck, 2012). We acknowledge that the difference between forward and reverse titrations may preclude a direct meaningful comparison (Hawkes et al., 2013a). Nevertheless, in both the buoyant and non-buoyant plume samples over Burke, we observed a trend of decreasing $\log K'_{FeL}$ with increasing DFe and [L] (Fig. 7). This trend suggests that weak ligands might be important for keeping Fe in the dissolved phase supporting the ideas and data interpretations discussed above. However, there is no correlation between $\log K'_{FeL}$ and DFe in the plumes over the high-temperature Perseverance field, consistent with previous reports of Hawkes et al. (2013a) and Wang et al. (2019). A possible explanation is that the extensive Fe precipitation and transfer between different Fe speciation in plumes above high-temperature

venting sites may lead to the lack of correlation between log K'_{FeL} and DFe.

The close relationships between [TFe], [TMn] and [L] in both the buoyant and non-buoyant above Burke (Fig. S2) suggest that there was a hydrothermal source of ligands to the Burke plumes. Previously, it has been assumed that the Fe-binding ligands in the plumes might be likely derived from the diffuse fluids adjacent to the vent sites (Bennett et al., 2008; Hawkes et al., 2013a; Kleint et al., 2016; Wang et al. 2019). Lang et al. (2006) observed that dissolved organic carbon (DOC) concentrations in diffuse fluids (49 ± 9 μM) were elevated compared with background seawater (36 μM). Furthermore, high concentrations of DOC have also been found in the "pore-water" fluids of the microbial mat samples near the vents, ranging from 68.4 μM to 179.2 μM, compared to 40.1 ± 0.8 μM in the ambient deep water (Bennett et al., 2011). In addition, lower pH in the areas near to the hydrothermal vents would also result in increases in Fe-binding ligand and dissolved Fe concentrations (Gledhill et al., 2015; Hiemstra and Van Riemsdijk, 2006). However, the in-situ production of ligands by microbial activity within the plumes can't be excluded. We found that the organic ligand fractions of DFe ([L]/[DFe] in the buoyant plume over Burke except sample V2-26 are ~5% on average lower than those in non-buoyant plume. This is consistent with the study of Bennett et al. (2011) on microbial carbon production in hydrothermal plumes at the Loihi seamount near Hawaii, which is also a low-temperature (42.7 ~ 50.7 °C) venting field. They observed a ~10% increase in DOC within plumes relative to the background DOC. As the non-buoyant plumes disperse away from venting sites, microbes may exert greater influence on the distributions of Fe species by producing a variety of organic ligands such as siderophores that dissolve solid-phase Fe minerals (Li et al., 2014). Recently, Hogle et al. (2016) directly observed production of strong and

weak Fe-binding ligands during 6 days of Fe spike incubation experiments, although it was conducted under incident light using subsurface water. Future studies should aim to investigate if microbial activities contribute to the Fe ligand pool as the plumes disperse into the deep sea.

There is another possibility that the low-temperature (< 51 °C) hydrothermal fluids of Burk vent might supply some Fe-binding ligands. Previous studies have identified large amounts of extractable organic compounds in the warm (≤ 91 °C) and alkaline fluids from the Lost City hydrothermal field, Mid-Atlantic Ridge (Lang et al., 2010; McCollom et al., 2015).

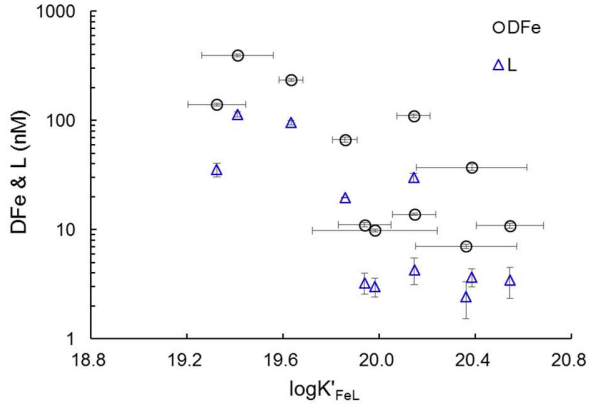

Fig. 7. The trend in $logK'_{FeL}$ with DFe and ligand concentrations. Error bars represent ±1 standard deviation of two replicate analyses. The standard deviation of $logK'_{FeL}$ was only shown on symbol circles.

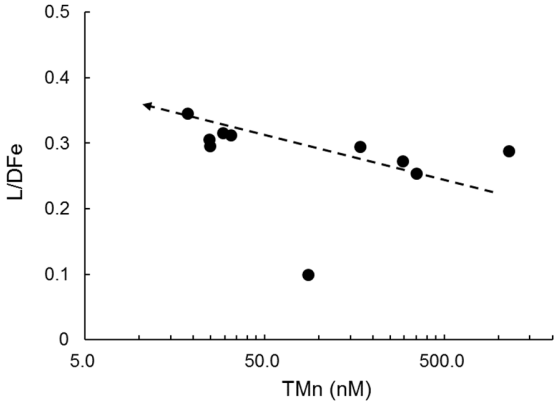

Fig. 8. L/DFe changes in the plume samples above Burke (except sample V2-26).

Along the southern segment, [L] in plume samples over Perseverance field and diffuse flow areas were not correlated to Fe species and TMn, which might be attributed to different hydrothermal sources of these plume waters and influence of ambient seawater. [L] in these samples was < 12.1 nM although TFe and DFe concentrations were still high. This may be due to the decline in activity of the Perseverance field where many dead chimneys were found, although the fluid temperature was still 265.7 °C (Baker et al., 2017; Butterfield et al., 2017; Chadwick et

458 al., 2018). Thus, less Fe-binding ligands were released into the plume. Similarly, it is also unlikely
459 for the diffuse flow plumes over newly erupted pillow lava lacking in chemolithoautotrophic
460 microorganisms and macrofauna to have high concentrations of ligands (Butterfield et al., 2017;
461 Chadwick et al., 2018).

462 However, for all the plume samples, DFe was 29.0 ± 9.3% (on average) organically complexed.
463 The remainder of DFe should be present as truly soluble and colloidal Fe oxyhydroxides and
464 sulfides. This is consistent with previous observations in high-temperature hydrothermal plumes
465 where most of the vented Fe forms nonexchangeable inorganic Fe (Fitzsimmons et al., 2017;
466 Hawkes et al., 2013a; Kleint et al., 2016; Wang et al., 2019). Notably, organically complexed Fe
467 composed 57.5 ± 15.6% of the Fe_{Lab} fraction (Table S2), confirming previous observations that the
468 organic ligands might control Fe_{Lab} and DFe distributions in hydrothermal plumes. Ligand-bound
469 Fe may play an important role in the distal transport of Fe in hydrothermal plumes to the broader
470 ocean, thus influencing oceanic Fe biogeochemistry.

471 **6. CONCLUSIONS**

472 In this study, we reported the differences of Fe speciation and distributions of Fe-binding
473 ligands in hydrothermal plumes above the Mariana back-arc. Our results showed that there were
474 significant differences in Fe geochemical characteristics in the hydrothermal plumes over low- and
475 high-temperature vents and over diffuse venting fields. TFe had higher concentrations of DFe and
476 Fe_{Lab} in the plumes over the low-temperature Burke than that over the high-temperature
477 Perseverance, which may be related to the low-temperature venting and low concentration of H_2S

in Burke fluids. Samples from the diffuse flow over newly erupted lava had the highest proportion of DFe present as Fe_{Lab}, which was mainly composed of Fe oxyhydroxides and sulfides. The linear relationships between TFe, DFe, Fe_{Lab} and TMn in the buoyant plumes above Burke show a simple conservative mixing between the plume and ambient seawater.

The characteristics of Fe-binding ligands in plumes depended on the type of seafloor hydrothermal venting, where the high ligand concentrations were likely derived from the diffuse flow and in-situ microbial carbon production. The decreasing of $logK'_{FeL}$ with increasing DFe and [L] in plume over Burke indicates the importance of weak ligands in stabilizing hydrothermal Fe. In all the plume samples, ligand bound Fe constituted more than half of the Fe_{Lab} fraction, which allowed Fe to remain dissolved in the deep ocean. We recommend future investigations on Fe speciation in low-temperature venting fields to better understand Fe biogeochemical behaviors in hydrothermal systems.

ACKNOWLEDGEMENT

The authors would like to thank all participants and the crews of the R/V Falkor for the FK151121 cruise. In particular, we thank Edward Baker and David Butterfield for their assistance in sampling and analysis during this cruise. We sincerely thank three anonymous reviewers and editors whose insightful comments have greatly improved the manuscript. This work was supported by National Natural Science Foundation of China (No. 41376048, 40976025), National Basic Research Program (973 Program) (No. 2012CB417300) and the Fundamental Research Funds for the Central Universities (22120180261). The seagoing effort was funded by NOAA's

Ocean Exploration Program and the Pacific Marine Environmental Laboratory through the Earth Ocean Interactions program. This is PMEL publication 4727 and JISAO publication 2018-0168.

APPENDIX A. SUPPLEMENTARY INFORMATION

Supplementary data to this article can be found online.

REFERENCES

Anderson M. O., Chadwick W. W. Jr., Hannington M. D., Merle S. G., Resing J. A., Baker E. T., Butterfield D. A., Walker S. L. and Augustin N. (2017) Geological interpretation of volcanism and segmentation of the Mariana back-arc spreading center between 12.78°N and 18.38°N. *Geochem. Geophys. Geosyst.* **18**, 2240-2274.

Ardyna M., Lacour L., Sergi S., d'Ovidio F., Sallée J. B., Rembauville M., Blain S., Tagliabue A., Schlitzer R., Jeandel C. and Arrigo K. R. (2019) Hydrothermal vents trigger massive phytoplankton blooms in the Southern Ocean. *Nat. Commun.* **10**: 2451.

Baker E. T., Resing J. A., Haymon R. M., Tunnicliffe V., Lavelle J. W., Martinez, F., Ferrini V., Walker S. L. and Nakamura K. (2016) How many vent fields?. New estimates of vent field populations on ocean ridges from precise mapping of hydrothermal discharge locations. *Earth Planet. Sci. Lett.* **449**, 186–196.

Baker E. T., Walker S. L., Resing J. A., Chadwick W. W., Merle S. G., Anderson M. O., Butterfield D. A., Buck N. J. and Michael S. (2017) The effect of arc proximity on hydrothermal activity along spreading centers: new evidence from the Mariana back arc (12.7°N-18.3°N). *Geochem. Geophys. Geosyst.* **18**, 4211-4228.

Beaulieu S. E., Baker E. T. and German C. R. (2015) Where are the undiscovered vents on oceanic spreading ridges? *Deep-Sea Res., Part II* **121**, 202-212.

522 Bemis K., Lowell R. P. and Farough A. (2012) Diffuse flow on and around hydrothermal vents at
523 mid-ocean ridges. *Oceanography* 25(1):182–191.
524 Bennett S. A., Achterberg E. P., Connelly D. P., Statham P. J., Fones G. R. and German, C. R. (2008)
525 The distribution and stabilisation of dissolved Fe in deep-sea hydrothermal plumes. *Earth*
526 *Planet. Sci. Lett.* **270**, 157-167.
527 Bennett S. A., Rouxel O. J., Schmidt K., Garbe-Schönberg D., Statham, P. J. and German C. R.
528 (2009) Iron isotope fractionation in a buoyant hydrothermal plume, 5 deg S Mid-Atlantic Ridge.
529 *Geochim. Cosmochim. Acta* **73**, 5619-5634.
530 Bennett S. A., Hansman R. L., Sessions A. L., Nakamura K. and Edwards K. J. (2011) Tracing iron-
531 fueled microbial carbon production within the hydrothermal plume at the Loihi seamount,
532 *Geochim. Cosmochim. Acta* **75**, 5526-5539.
533 Boyd P. W., Ellwood M. J., Tagliabue A. and Twining B. S. (2017) Biotic and abiotic retention,
534 recycling and remineralization of metals in the ocean. *Nat. Geosci.* **10**, 167-173.
535 Buck K. N., Lohan M. C., Berger C. J. M. and Bruland, K. W. (2007) Dissolved iron speciation in
536 two distinct river plumes and an estuary: Implications for riverine supply. *Limnol. Oceanogr.*
537 **52**, 843-855.
538 Buck K. N., Sohst B. and Sedwick P. N. (2015) The organic complexation of dissolved iron along
539 the U.S. GEOTRACES (GA03) North Atlantic Section. *Deep-Sea Res. II* **116**, 152-165.
540 Bundy R. M., Biller D. V., Buck K. N., Bruland K. W. and Barbeau, K. A. (2014) Distinct pools of
541 dissolved iron-binding ligands in the surface and benthic boundary layer of the California
542 Current. *Limnol. Oceanogr.* **59**, 769-787.
543 Bundy R. M., Abdulla H. A., Hatcher P. G., Biller D. V., Buck K. N. and Barbeau K. A. (2015)
544 Iron‐binding ligands and humic substances in the San Francisco Bay estuary and estuarine‐
545 influenced shelf regions of coastal California. *Mar. Chem.* **173**, 183-194.
546 Butterfield D. and Shipboard Scientific Party. (2017) Hydrothermal hunt at the Mariana back-arc,
547 Leg 2, in Cruise Report for FK161129 on RV Falkor, Seattle, Wash.
548 Campbell A. C., Edmond J. M., Colodner D., Palmer M. R. and Falkner, K. K. (1987) Chemistry

549 of hydrothermal fluids from the Mariana Trough backarc basin in comparison to mid-ocean
550 ridge fluids. EOS Trans. AGU **68**, 1531.
551 Chadwick W. W. Jr, Merle S. G., Baker E. T., Walker S. L., Resing J. A., Butterfield D. A., Anderson
552 M. O., Baumberger T. and Bobbitt A. M. (2018) A Recent Volcanic Eruption Discovered on the
553 Central Mariana Back-Arc Spreading Center. *Front. Earth Sci.* **6**, 172.
554 Coale, K. H., Johnson, K. S., Fitzwater, S. E., Gordon, R. M., Tanner, S., Chavez, F. P., et al. (1996).
555 A massive phytoplankton bloom induced by an ecosystem scale iron fertilization experiment
556 in the equatorial Pacific Ocean. *Nature*, **383,** 495 – 501.
557 Croot P. L. and Heller M. I. (2012) The importance of kinetics and redox in the biogeochemical
558 cycling of iron in the surface ocean. *Front. Microbio.* **3**: 219.
559 Croot P. L. and Johansson M. (2000) Determination of iron speciation by cathodic stripping
560 voltammetry in seawater using the competing ligand 2-(2-thiazolylazo)-p-cresol (TAC).
561 *Electroanalysis*, **12**, 565-576.
562 Dick G. J., Clement B. G., Webb S. M., Fodrie F. J., Bargar J. R. and Tebo B. M. (2009) Enzymatic
563 microbial Mn(II) oxidation and Mn biooxide production in the Guaymas Basin deep-sea
564 hydrothermal plume. *Geochim. Cosmochim. Acta* **73**, 6517-6530.
565 Field M. P. and Sherrell R. M. (2000) Dissolved and particulate Fe in a hydrothermal plume at 9°45'
566 N, East Pacific Rise: slow Fe(II) oxidation kinetics in Pacific plumes. *Geochim. Cosmochim.*
567 *Acta* **64**, 619-628.
568 Fitzsimmons J. N., Boyle E. A. and Jenkins W. J. (2014) Distal transport of dissolved hydrothermal
569 iron in the deep South Pacific Ocean. *Proc. Natl. Acad. Sci. USA* **111**, 16654-16661.
570 Fitzsimmons J. N., John S. G., Marsay C. M., Hoffman C. L., Nicholas S. L., Toner B. M., German
571 C. R. and Sherrell R. (2017) Iron persistence in a distal hydrothermal plume supported by
572 dissolved-particulate exchange. *Nat. Geosci.* **10**, 195-201.
573 Fornari D. J. and Embley R.W. (1995) Tectonic and volcanic controls on hydrothermal processes
574 at the mid-ocean ridge: An overview based on near-bottom and submersible studies. In *Physical,*
575 *Chemical, Biological, and Geological Interactions within Seafloor Hydrothermal Systems* (S.

E. Humphris, R. A. Zierenberg, L. Mullineaux and R. Thomson, Geophys. Union, pp. l-46.

Gamo T., Tsunogai U., Ishibashi J., Masuda H. and Chiba H. (1997) Chemical characteristics of hydrothermal fluids from the Mariana Trough. JAMSTEC J. *Deep Sea Res. Special volume*, 69-74.

German C. R., Casciotti K. A., Dutay J. C., Heimbürger L. E., Jenkins W. J., Measures C. I., Mills R. A., Obata H., Schlitzer R., Tagliabue A., Turner D. R. and Whitby H. (2016) Hydrothermal impacts on trace element and isotope ocean biogeochemistry. *Phil. Trans. R. Soc. A* **374**: 20160035.

Gerringa L. J. A., Rijkenberg M. J. A., Wolterbeek H. T., Verburg T. G., Boye M. and deBaar H. J. W. (2007) Kinetic study reveals weak Fe-binding ligand, which affects the solubility of Fe in the Scheldt estuary. *Mar. Chem.* **103**, 30-45.

Gledhill M. and Buck K. N. (2012) The organic complexation of iron in the marine environment: a review. *Front. Microbiol.* **3**, 1-17.

Gledhill M., Achterberg E. P., Li K., Mohamed K. N. and Rijkenberg M. J. A. (2015) Influence of ocean acidification on the complexation of iron and copper by organic ligands in estuarine waters. *Mar. Chem.* **177**, 421-433.

Gledhill M. and Gerringa L. J. A. (2017) The Effect of Metal Concentration on the Parameters Derived from Complexometric Titrations of Trace Elements in Seawater-A Model Study. *Front. in Ma. Sci.* **4**, 254.

Hawkes J. A., Connelly D. P., Gledhill M. and Achterberg E. P. (2013a) The stabilisation and transportation of dissolved iron from high temperature hydrothermal vent systems. *Earth Planet. Sci. Lett.* **375**, 280-290.

Hawkes J. A., Connelly D. P., Rijkenberg M. J. A. and Achterberg E. P. (2014) The importance of shallow hydrothermal island arc systems in ocean biogeochemistry. *Geophys. Res. Lett.* **41**, 942-947.

Hawkes J. A., Gledhill M., Connelly D. P. and Achterberg E. P. (2013b) Characterisation of iron binding ligands in seawater by reverse titration. *Anal. Chim. Acta* **766**, 53-60.

603 Hessler R. R. and Lonsdale P. F. (1991) Biogeography of Mariana Trough hydrothermal vent
604 communities. *Deep Sea Research Part A* **38**, 185-199.
605 Hiemstra, T. and Van Riemsdijk W. H. (2006). Biogeochemical speciation of Fe in ocean
606 water. *Mar. Chem.* ***102***, 181-197.
607 Hogle S. L., Bundy R. M., Blanton J. M., Allen E. and Barbeau K. A. (2016) Copiotrophic marine
608 bacteria are associated with strong iron-binding igand production during phytoplankton blooms.
609 *Limnol. Oceanogr.: Letters* **1**, 36-43.
610 Ishibashi J. I., Tsunogai U, Toki T., Ebina N., Gamo T., Sano Y., Masuda H. and Chiba H. (2015)
611 Chemical composition of hydrothermal fluids in the central and southern Mariana Trough
612 backarc basin. *Deep. Sea Res. II*, **121**, 126-136.
613 James R. H. and Elderfield H. (1996) Dissolved and particulate trace metals in hydrothermal
614 plumes at the Mid-Atlantic Ridge. *Geophys. Res. Lett.* **23**, 3499-3502.
615 Kleint C., Hawkes J. A., Sander S. and Koschinsky A. (2016) Voltammetric Investigation of
616 Hydrothermal Iron Speciation. *Front. Mar. Sci.* **3**: 75.
617 Laglera L. M. and Van den Berg, C. M. G. (2009) Evidence for geochemical control of iron by
618 humic substances in seawater. *Limnol. Oceanogr.* **54**, 610-619.
619 Laglera L. M., Battaglia G. and Van den Berg C. M. G. (2011) Effect of humic substances on the
620 iron speciation in natural waters by CLE/CSV. *Mar. Chem.* **127**, 134-143.
621 Lang S. Q., Butterfield D. A., Lilley M. D., Johnson H. P. and Hedges J. I. (2006) Dissolved organic
622 carbon in ridge-flank and ridge-axis environments. *Geochim Cosmochim Acta* **70**, 3830–3842.
623 Lang S. Q., Butterfield D. A., Schulte M., Kelley D. S. and Lilley M. D. (2010) Elevated
624 concentrations of formate, acetate and dissolved organic carbon found at the Lost City
625 hydrothermal field. *Geochim. Cosmochim. Acta* **74**, 941-952.
626 Li M., Toner B. M., Baker B. J., Breier J. A., Sheik C. S. and Dick G. J. (2014) Microbial iron
627 uptake as a mechanism for dispersing iron from deep-sea hydrothermal vents. *Nat. Commun.*
628 **5**: 3192.
629 Liu X. and Millero F. J. (2002) The solubility of Fe in seawater. *Mar. Chem.* **77**, 43-54.

630 Lough A. J. M., Homoky W. B., Connelly D. P., Comer-Warner S. A., Nakamura N., Abyaneh M.
631 K., Kaulich B. and Mills R. A. (2019) Soluble iron conservation and colloidal iron dynamics
632 in a hydrothermal plume. *Chem. Geol.* **511**, 225-237.
633 Martinez F. and Taylor B. (2003) Controls on back‐arc crustal accretion: Insights from the Lau,
634 Manus and Mariana basins. In *Intra-oceanic subduction systems: Tectonic and magmatic*
635 *processes* (eds. R. D. Larter and P. T. Leat), Geological Society of London, London, pp. 19-54.
636 McCollom T. M., Seewald J. S. and German C. R. (2015) Investigation of extractable organic
637 compounds in deep-sea hydrothermal vent fluids along the Mid-Atlantic Ridge. *Geochim.*
638 *Cosmochim. Acta* **156**, 122-144.
639 Measures C. I., Yuan J. and Resing J. A. (1995) Determination of iron in seawater by flow injection
640 analysis using in-line preconcentration and spectrophotometric detection. Mar. Chem. 50, 3-12.
641 Millero F. J. and Pierrot D. (2007) The activity coefficients of Fe(III) hydroxide complexes in NaCl
642 and $NaClO_4$ solutions. *Geochim. Cosmochim. Acta* **71**, 4825-4833.
643 Mottl M. J. (2003) Partitioning of energy and mass fluxes between mid-ocean ridge axes and flanks
644 at high and low temperature. In *Energy and mass transfer in marine hydrothermal systems* (eds.
645 P. Halbach, V. Tunnicliffe and J. Hein), Dahlem University Press, Berlin, pp. 271-286.
646 Mottl M. J. and McConachy T. F. (1990) Chemical processes in buoyant hydrothermal plumes on
647 the East Pacific Rise near 21°N. *Geochim. Cosmochim. Acta*, **54**, 1911-1927.
648 Nishioka J., Obata H. and Tsumune D. (2013) Evidence of an extensive spread of hydrothermal
649 dissolved iron in the Indian Ocean. *Earth Planet. Sci. Lett.* **361**, 26-33.
650 Nuester J. and Van den Berg C. M. G. (2005) Determination of metal speciation by reverse titrations.
651 *Anal. Chem.* **77**, 11-19.
652 Resing J. A. and Mottl M. J. (1992) Determination of manganese in seawater using flow injection
653 analysis with on-line preconcentration and spectrophotometric detection. *Anal. Chem.* **64**,
654 2682-2687.
655 Resing J. A, Sedwick P. N, German C. R., Jenkins W. K., Moffett J. W., Sohst B. M. and Tagliabue
656 A. (2015) Basin-scale transport of hydrothermal dissolved metals across the South Pacific

Ocean. *Nature* **523**, 200-203.

Resing J. A. and Shipboard Scientific Party. (2016) Hydrothermal hunt at Mariana back-arc, in Cruise Report for FK151121 on RV Falkor, Seattle, Wash.

Resing J. A., Baker E. T., Lupton J. E., Walker S. L., Butterfield D. A., Massoth G. J. and Nakamura K. (2009) Chemistry of hydrothermal plumes above submarine volcanoes of the Mariana Arc. *Geochem. Geophys. Geosyst.* **10**, Q02009, doi:10.1029/2008GC002141.

Rona P. A. and Trivett D. A. (1992) Discrete and diffuse heat transfer at ASHES vent field, Axial Volcano, Juan de Fuca Ridge. *Earth Planet. Sci. Lett.* **109**, 57-71.

Rue E. L. and Bruland K. W. (1995). Complexation of iron(III) by natural organic ligands as determined by a new competitive equilibration/adsorptive cathodic stripping voltammetry method. *Mar. Chem.* **50**, 117-138.

Saito M. A., Noble A. E., Tagliabue A., Goepfert T. J., Lamborg C. H. and Jenkins W. J. (2013) Slow-spreading submarine ridges in the South Atlantic as a significant oceanic iron source. *Nature Geosci.* **6**, 775-779.

Sander S. G. and Koschinsky, A. (2011) Metal flux from hydrothermal vents increased by organic complexation. *Nat. Geosci.* **4**, 145-150.

Sands C. M., Connelly D. P., Statham P. J. and German C. R. (2012) Size fractionation of trace metals in the Edmond hydrothermal plume, Central Indian Ocean. *Earth Planet. Sci. Lett.* **319-320**, 15-22.

Tagliabue A., Bopp L., Dutay J. C., Bowie A. R., Chever F., Jean-Baptiste P., Bucciarelli E., Lannuzel D., Remenyi T., Sarthou G., Aumont O., Gehlen M. and Jeandel C. (2010) Hydrothermal contribution to the oceanic dissolved iron inventory. *Nat. Geosci.* **3**, 252-256.

Tagliabue A. and Resing J. (2016) Impact of hydrothermalism on the ocean iron cycle. *Phil. Trans. R. Soc. A* **374**: 20150291.

Tagliabue A., Bowie A. R., Boyd P. W., Buck K. N., Johnson K. S. and Saito M. A. (2017) The integral role of iron in ocean biogeochemistry. *Nature* **543,** 51-59.

Town R. M. and Filella M. (2000) Dispelling the myths: is the existence of L1 and L2 ligands

necessary to explain metal ion speciation in natural waters? *Limnol. Oceanogr.* 45, 1341-1357.

Von Damm K. L., Edmond J. M., Grant B., Measures C. I., Walden B. and Weiss R. F. (1985) Chemistry of submarine hydrothermal solutions at 21°N, East Pacific Rise, *Geochim. Cosmochim. Acta*, **49**, 2197-2220.

Wang H., Yan Q., Yang Q., Ji F., Wong K. H. and Zhou H. (2019) The size fractionation and speciation of iron in the Longqi hydrothermal plumes on the Southwest Indian Ridge. *J. Geophys. Res.-Oceans* **124**, 4029-4043.

Wang H., Yang Q., Ji F., Lilley M. D. and Zhou H. (2012) The geochemical characteristics and Fe(II) oxidation kinetics of hydrothermal plumes at the Southwest Indian Ridge. *Mar. Chem.* **134 - 135**, 29-35.

Yücel M., Gartman A., Chan C. S. and Luther G. W. (2011) Hydrothermal vents as a kinetically stable source of iron-sulphide-bearing nanoparticles to the ocean. *Nat. Geosci.* **4**, 367-371.